RP Current Trends In Applied Sciences
Vol. 2, No. 2 (April – June 2023) pp. 34–38
e-ISSN: 2583-7486

RESEARCH PLATEAU PUBLISHERS

Cite this article: N. Singh, Effects of NiO, CuO, and MnO nanoparticles on the structural, morphological, and electrical properties of a porous carbon matrix synthesized by the sol-gel method, *RP Cur. Tr. Appl. Sci.* **2** (2023) 34–38.

Original Research Article

Effects of NiO, CuO, and MnO nanoparticles on the structural, morphological, and electrical properties of a porous carbon matrix synthesized by the sol-gel method

Navneet Singh*
Department of Physics, Rajiv Gandhi Government College for Women, Bhiwani – 127021, Haryana, India
*Corresponding author, E-mail: ndhanda16@gmail.com

ARTICLE HISTORY
Received: 12 Jan. 2023
Revised: 22 April 2023
Accepted: 26 April 2023
Published online: 2 May 2023

KEYWORDS
Carbon matrix; Inorganic nanopowders; Nanocomposite; Electrical conductivity; Hopping conduction mechanism.

ABSTRACT
In this paper, we describe the sol-gel approach for the synthesis of various hybrid nanocomposites. In order to incorporate the nanopowder oxides of nickel (NiO), copper (CuO), and manganese (MnO) in the porous carbon matrix based on pyrogallol and formaldehyde (PF), we employed picric acid as a catalyst. The materials were then dried and heated for two hours at 650°C pyrolysis temperature before being characterised using various structural and electrical methods. The inclusion of inorganic nanoparticles increased the crystallisation of several nanocomposites with the presence of a graphite phase, according to the X-ray diffraction (XRD) spectra. The size of the graphite nanoparticles is dependent on the amount of inorganic oxide contained, as shown by the TEM images. We see from the electrical experiments that the existence of graphite nanoparticles is related to electrical conduction. The influence of the hopping conduction mechanism in these nanocomposites is explained by the fluctuation of the electrical conductivity and the relaxation time with measurement temperature, which ranges between 80 and 300 K.

1. Introduction

Many promising materials, including those for the adsorption and separation of greenhouse gases, have been developed using the porous carbon matrix [1, 2]. In fact, this matrix has a distinct pore structure, good stability, and low preparation costs [3, 4]. The porous carbon matrix based on pyrogallol-formaldehyde (PF) is one of the organic gels known for its intriguing prospective features dependent on the synthesis conditions [5]. Different hybrid organic/inorganic nanocomposites are created when inorganic nanoparticles are implanted in a porous carbon matrix [6–8]. These hybrid nanocomposites have received a lot of interest from researchers recently, whether from an applied or fundamental perspective [9, 10]. Numerous applications, such as solar cells [11], hydrogen storage [12], negatronic devices [13], and electrochemical devices such sensors [14], make substantial use of them. In fact, the inorganic nanoparticles are useful materials that are both scientifically and technologically intriguing. They have a wide range of features that touch on almost every field of physics and materials science. Due to the significance of their applications in biology, the environment, analytical chemistry, and physics, they are crucial for research [15]. The efficacy of nanomaterials when used as biomimetic membranes to detect proteins and sustain their activity is actually improved by these nanoparticles, which exhibit high surface-to-volume ratios, low toxicity, high chemical stability, and rapid electron transfer abilities [16, 17]. However, the introduction of inorganic nanoparticles into a porous carbon matrix paved the way for a brand-new class of materials with distinctive electrical and optical characteristics, making them appealing for usage in fields including optoelectronics [18], sensor design [19, 20], and catalysis [21].

The varied electrical properties of the hybrid nanocomposites are mostly determined by the interfacial interaction between the inorganic nanoparticles and the PF porous matrix. It has been largely accepted that the development of distinctive interface regions between carbon matrix and inorganic nanoparticles is what first caused electrical transport phenomena. Enhancing conductivity and other electrical characteristics of these nanocomposites depends heavily on the interfaces. Therefore, the primary objectives of this research are to synthesise, characterise, and comprehend the electrical conduction mechanism in these materials.

2. Experimental

2.1 Preparation

Sol-gel synthesis has been used to create PF porous carbon matrix and PF/NiO, PF/CuO, and PF/MnO nanocomposites. First, methanol was used to dissolve the precursors for manganese (II) chlorid tetrahydrate, copper (II) acetylacetonate, and nickel (II) chlorid ($NiCl_2$,$6H_2O$). The solutions were then deposited in an autoclave and dried in supercritical ethyl alcohol after 15 minutes of magnetic stirring at room temperature. The resulting nanopowders were blended with a mass proportion of 5% in pyrogallol (P), formaldehyde (F), and water solution after being annealed at 500°C in air for two hours. The process was then activated using picric acid. Second, the resultant wet gel was dried over a 15-day period at 50°C. The produced xerogel monolith is dried with a heating

rate of 10° C./day up to 150°C in an effort to prevent any shrinking.

Finally, using a typical drying process similar to that used for the PF matrix, the various nanocomposites were obtained. In our case, all samples underwent a two-hour heat treatment at 650°C with a heating rate of 5°C/min in a tube furnace with a regulated nitrogen environment. After natural cooling, we prepared the samples in a parallelepipedal form (12×6×3) mm^3 with an ohmic contact in silver paint on two parallel faces for the electrical measurements.

2.2 Characterization

The collected samples were examined using an X-ray diffractometer (XRD) from a Bruker D5005 equipped with CoKα radiation. We employ a JEOL-100C TEM for the morphological examination and an Agilent-4294A impedance analyzer for the measurements of electrical conductivity and relaxation time for frequencies from 40 Hz to 10 MHz. A Janis Corporation VPF-100 cryostat that was cooled with liquid nitrogen produced the fluctuation in measurement temperature.

3. Results and discussion

The XRD patterns of the produced PF matrix and several nanocomposites are displayed in Figure 1. Two significant diffraction peaks at 24° and 42°, corresponding to the (002) and (100) planes typical of amorphous carbon, were identified in the PF matrix. On the other hand, the various nanocomposites have crystallised. It is evident that the PF/NiO nanocomposite exhibits three separate metallic nickel reflection peaks, the PF/CuO nanocomposite exhibits three distinct metallic copper reflection peaks, and the PF/MnO nanocomposite exhibits two phases of manganese oxide, MnO, and metallic manganese, Mn. The PF matrix and other nanocomposites' crystallite sizes were determined using Scherrer's equation Eq. (1) [23]:

$$G = \frac{0.9\lambda}{\beta \cos\theta_B}, \qquad (1)$$

where θ_B is the maximum Bragg diffraction peak and B is the line width at half maximum and λ is the X-ray wavelength. According to the diameter of the crystallites estimated using Eq. (1), the average value of graphite crystallites was found to be approximately 2 nm for the PF matrix, 3.5 nm, 5 nm, and 15 nm for the PF/NiO, PF/CuO, and PF/MnO nanocomposites, respectively. The typical size of the other crystallite kinds, including Ni, Cu, Mn, and MnO, ranges from 12 nm to 50 nm. These findings suggest that the incorporation of inorganic nanoparticles into the carbon matrix when subjected to temperatures of pyrolysis of 650°C results in a change in the crystalline properties of various nanocomposites in comparison to those of the PF matrix.

Using Eq. (2) and the value of the resistance R acquired by the impedance analyzer at low frequency, the electrical conductivity of the tested material was calculated.

$$\sigma = L/RS \qquad (2)$$

where L is the pellet's thickness and S is the electrode's contact area. The presence of a linear form in the change of electrical conductivity versus $T^{-1/4}$ (Figure 3) indicates that the 3D Godet-Variable Range Hopping (3D-GVRH) mechanism may be appropriate to characterize the temperature dependence of conductivity [24].

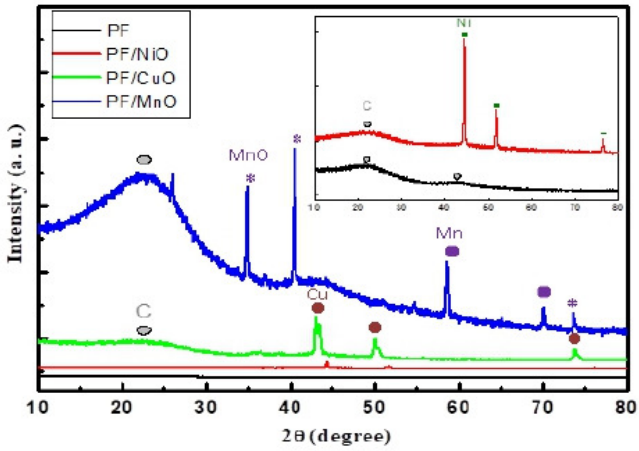

Figure 1: XRD patterns of the all prepared samples.

The TEM observations for the materials under examination are shown in Figure 2. These photos demonstrate how the incorporated oxide changed the nanoparticles' sizes. It discovered that all of the samples' nanoparticles had clumped together. The PF/MnO nanocomposite produced the biggest size, while the PF organic matrix produced the smallest. These micrographs correspond to the XRD findings.

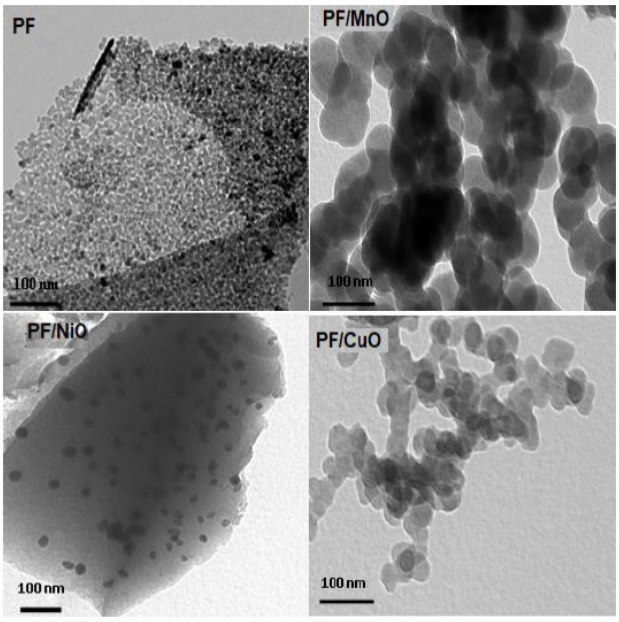

Figure 2: TEM micrographs of the different prepared samples.

When the charge carrier interaction is ignored in this model, the dc conductivity is given by Eq. (3):

$$\sigma_{dc} = \sigma_0 \exp\left(-\frac{T_0}{T}\right)^{1/4}, \qquad (3)$$

where σ_0 is a pre-exponential factor, T is the measurement temperature. T_0 is the Godet characteristic temperature, which is calculated using Eq. (4) [25]:

$$T_0 = 310\frac{\alpha^3}{N(E_F)k_B}, \quad (4)$$

where $N(E_F)$ is the density of states, k_B is the constant of Boltzmann and $1/\alpha$ is the carrier localization length.

The variability in electrical conductivity and density of states for the different samples at room measurement temperature is shown in Figure 4. From those two curves, the density of states and electrical conductivity are inversely correlated. Indeed, with minimum conductivity, $N(E_F)$ achieves the greatest value in the PF matrix. $N(E_F)$ tends to a minimal value with a maximum conductivity in the PF/MnO nanocomposite.

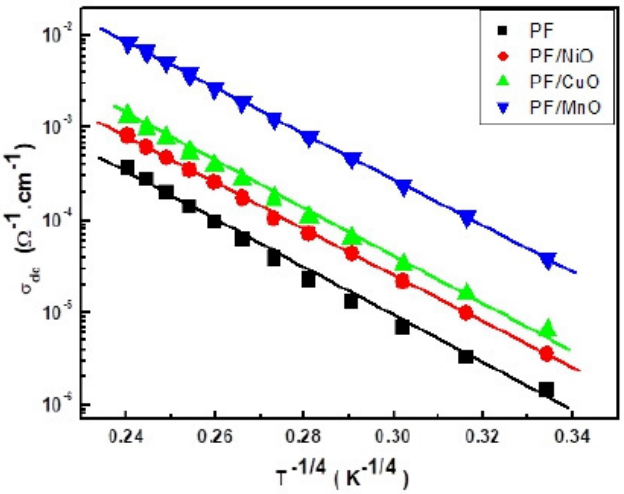

Figure 3: Variation of the dc conductivity versus $T^{-1/4}$.

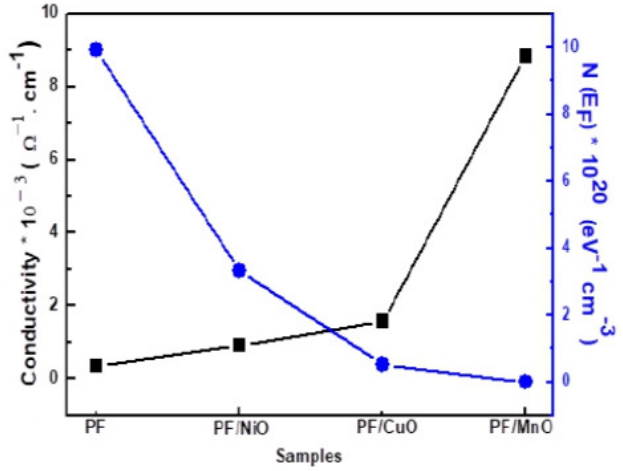

Figure 4: Electrical conductivity and density of states for the all samples.

In order to pinpoint the cause of the rise in graphite's electrical conductivity, we have displayed the variance in electrical conductivity and the size of the crystallites for several samples in Figure 5. The electrical conductivity and the size of graphite crystallites are proportional, as seen by the two curves. This demonstrates that the electrical conductivity of graphite nanoparticles is caused by their size.

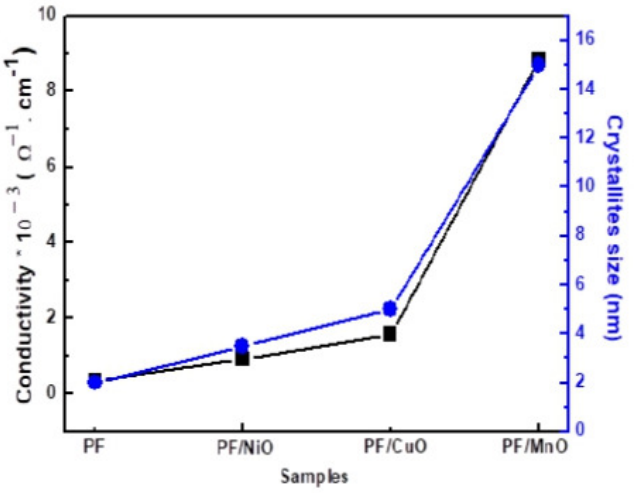

Figure 5: Electrical conductivity and crystallites size of graphite for the different samples.

Electrical conductivity is plotted on a semi-log scale in Figure 6 as a function of 1000/T. Our materials' increased electrical conductivity as measurement temperature rises is evidence of their semiconductor behaviour characteristics. The curves exhibit activation temperature dependency as predicted by Eq. (5) [26]:

$$\sigma = A\exp\left(-\frac{E_a}{k_B T}\right), \quad (5)$$

where activation energy, E_a and A is the pre-exponential factor. The activation energies determined by the linear fit at high temperature for the PF, PF/NiO, PF/CuO, and PF/MnO samples are, respectively, 101, 92, 90, and 81 meV, according to Eq. (5). Lower activation energy values were obtained in our samples as a result of the integration of inorganic nanoparticles into the carbon matrix PF by reducing the space between graphite particles and favourably increasing electrical conductivity.

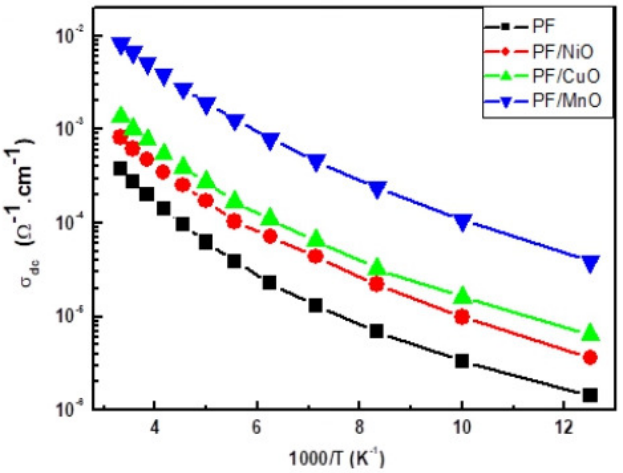

Figure 6: Variation of the dc conductivity versus 1000/T.

From 40 Hz to 100 MHz of frequencies were used to measure the impedance. We used the variation of the imaginary portion of the impedance as a function of frequency to estimate the relaxation time for measurement temperatures between 80 and 300 K.

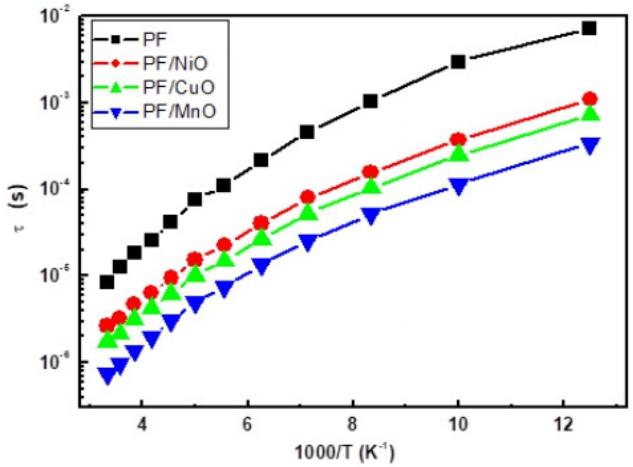

Figure 7: Variation of the relaxation time versus 1000/*T*.

Figure 7 depicts the variation in relaxation time as a function of the inverse of measurement temperature. The curves illustrate activation temperature dependency in accordance with Eq. (6).

$$\tau = \tau_0 \exp\left(\frac{E_a^{'}}{k_B T}\right), \qquad (6)$$

where τ_0 is the pre-exponential factor and $E_a^{'}$ is the activation energy of relaxation time. According to Eq. (6), the values of $E_a^{'}$ for PF, PF/NiO, PF/CuO, and PF/MnO samples are 104, 94, 93, and 84 meV, respectively. These results are in good agreement with electrical conductivity-derived values, demonstrating that hopping conduction dominates in both dc and ac modes.

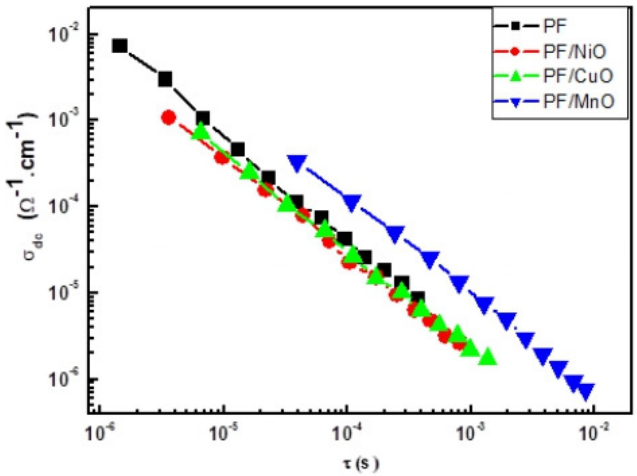

Figure 8: Variation of dc conductivity versus the relaxation time.

In a log-log scale, Figure 8 displays the change of electrical conductivity vs relaxation time. For the numerous samples under investigation, the measured linearity supports the hypothesis that conductivity and relaxation time are correlated. In materials with hopping charge transport characteristics, this proportionality might be observed [27, 28].

4. Conclusions

A porous carbon matrix based on pyrogallol-formaldehyde synthesised using the sol-gel method was investigated to see how NiO, CuO, and MnO nanoparticles affected its structural, morphological, and electrical properties. The structural and morphological characterizations demonstrate how the incorporating metallic oxide affects the nanoparticle size. The variation in conductivity caused by the injected metallic oxide is explained by the size of the graphite nanoparticles. The hopping conduction process rules in both the dc and ac regimes.

References

[1] D. Jayne, Y. Zhang, S. Haji, C. Erkey, Dynamics of removal of organosulfur compounds from diesel by adsorption on carbon aerogels for fuel cell applications, *Int. J. Hydrogen Energy* **30** (2005) 1287-1293.

[2] K.Y. Kang, B.I. Lee, J.S. Lee, Hydrogen adsorption on nitrogen doped carbon xerogels, *Carbon* **47** (2009) 1171-1180.

[3] K.P. Wang, H. Teng, The performance of electric double layer capacitors using particulate porous carbons derived from PAN fiber and phenol-formaldehyde resin, *Carbon* **44** (2006) 3218-3225.

[4] F.J. Maldonado-Hodar, C. Moreno-castilla, A.F. Perez-Dadenas, Surface morphology, metal dispersion, and pore texture of transition metal-doped monolithic carbon aerogels and steamactivated derivatives, *Microporous Mesoporous Mater* **69** (2004) 119-125.

[5] L. El Mir, S. Kraiem, M. Bengagi, E. Elaloui, A. Ouderni, S. Alaya, Synthesis and characterization of electrical conducting nanoporous carbon structures, *Physica B* **395** (2007) 104-110.

[6] N. Ben Mansour, L. El Mir, Study of carbon/copper nanocomposite synthesized by sol-gel method, *Journal of Materials Science: Materials in Electronics* **27** (2016) 11682-11690.

[7] N. Ben Mansour, L. El Mir, Influence of the nickel oxide nanoparticles content on the electrical properties of carbon/nickel nanocomposites, *Journal of Materials Science: Materials in Electronics* **28** (2017) 11284-11291.

[8] N. Ben Mansour, L. El Mir, Origin of dc and ac electric transport phenomena in carbon/manganese oxide nanocomposite, *Journal of Solid State Sciences* **85** (2018) 38-47.

[9] A. Okada, A. Usuki, The chemistry of polymer-clay hybrids, *Mater. Sci. Eng*. **3** (1995) 109-115.

[10] E.P. Giannelis, Polymer layered silicate nanocomposites, *Adv. Mater*. **8** (1996) 29-35.

[11] W.J.E. Beek, M.M. Wienk, M. Kemerink, X. Yang, R.A.J. Janssen, Hybrid zinc oxide conjugated polymer bulk heterojunction solar cells, *J. Phys. Chem. B* **109** (2005) 9505-9516.

[12] S.F. Wang, F. Xie, R.F. Hu, Sens, Carbon-coated nickel magnetic nanoparticles modified electrodes as a sensor for determination of acetaminophen, *Actuators B* **123** (2007) 495-500.

[13] N.A. Filinyuk, Proceedings of a USSR Scientific and Technical Conference on Devices with Negative Resistance and Integrated Converters on Their Basis, Baku, Russian (1991) 11.

[14] M. Zielinski, R. Wojcieszak, S. Monteverdi, M. Mercy, M.M. Bettahar, Hydrogen storage in nickel catalysts supported on activated carbon, *Int. J. Hydrogen Energy* **32** (2007) 1024-1032.
[15] G. Malandrino, S.T. Finocchiaro, R.T. Nigro. Free-standing copper(II) oxide nanotube arrays through an MOCVD template process, *Chem. Mater*. **16** (2004) 5559-5561.
[16] N. Chopra, V.G. Gavalas, L.G. Bachas, B.J. Hinds, L.G. Bachas, Functional one dimensional nanomaterials: applications in nanoscale biosensors, *Anal. Lett*. **40** (2007) 2067-2096.
[17] K. Kerman, M. Saito, S. Yamamura, Y. Takamura, E. Tamiya, Nanomaterial-based electrochemical biosensors for medical applications, *Trends Anal. Chem*. **27** (2008) 585-592.
[18] R.C. Jin, Y.W. Cao, C.A. Mirkin, K.L. Kelley, G.C. Schatz, J.G. Zheng, Photoinduced conversion of silver nanospheres to nanoprisms, *Science* **294** (2001) 1901-1906.
[19] M. Hjiri, R. Dahari, N. Ben Mansour, L. El Mir, M. Bonyani, A. Mirzaei, S.G. Leonardi, G. Neri, Electrochemical properties of a novel Ni-doped nanoporous carbon, *Materials Letters* **160** (2015) 452-455.
[20] S. Marini, N. Ben Mansour, M. Hjiri, R. Dhahri, L. El Mir, C. Espro, A. Bonavita, S. Galvagno, G. Neri, S.G. Leonardi, Non-enzymatic glucose sensor based on nickel/carbon composite, *Electroanalysis* **30** (2018) 728-733.
[21] D.M. Vriezema, M.C. Aragones, J.A.A.W. Elemans, J.J.L.M. Cornelissen, A.E. Rowan, R.J.M. Nolte, Self-assembled nanoreactors, *Chem. Rev*. **105** (2005) 1445-1490.
[22] L. El Mir, A. Amlouk, C. Barthou, S. Alaya, Synthesis and luminescence properties of ZnO/Zn 2SiO 4/SiO 2 composite based on nanosized zinc oxide-confined silica aerogels, *Physica B: Condensed Matter* **388** (2007) 412-417.
[23] H. Saeki, H. Tabata, T. Kawai, Magnetic and electric properties of vanadium doped ZnO films, *Solid State Commun*. **120** (2001) 439-443.
[24] C. Godet, Variable range hopping revisited: the case of an exponential distribution of localized states, *J. Non-Cryst. Solids*, **299** (2002) 333-338.
[25] C. Godet, Electronic localization and bandtail hopping charge transport, *Phys. Stat. Solidi B* **231** (2002) 499-511.
[26] N.F. Mott, E.A. Davis, Electronic Processes in Non-Crystalline Materials, Clarendon, Oxford (1979) 157.
[27] J.C. Dyre, The random free energy barrier model for ac conduction in disordered solids, *J. Appl. Phys*. 64 (1988) 2456-2468.
[28] H. Jhans, D. Kim, R.J. Rasmussen and J.M. Honig, ac-conductivity measurements on $La_2NiO_{4+\delta}$, *Physical review B* **54** (1996) 11224.